Cell

Upf1 Senses 3′UTR Length to Potentiate mRNA Decay

J. Robert Hogg[1,3,*] and Stephen P. Goff[1,2,3,*]
[1]Department of Biochemistry and Molecular Biophysics
[2]Department of Microbiology and Immunology
[3]Howard Hughes Medical Institute
College of Physicians and Surgeons, Columbia University, New York, NY 10032, USA
*Correspondence: jh2721@columbia.edu (J.R.H.), spg1@columbia.edu (S.P.G.)
DOI 10.1016/j.cell.2010.10.005

SUMMARY

The selective degradation of mRNAs by the nonsense-mediated decay pathway is a quality control process with important consequences for human disease. From initial studies using RNA hairpin-tagged mRNAs for purification of messenger ribonucleoproteins assembled on transcripts with HIV-1 3′ untranslated region (3′UTR) sequences, we uncover a two-step mechanism for Upf1-dependent degradation of mRNAs with long 3′UTRs. We demonstrate that Upf1 associates with mRNAs in a 3′UTR length-dependent manner and is highly enriched on transcripts containing 3′UTRs known to elicit NMD. Surprisingly, Upf1 recruitment and subsequent RNA decay can be antagonized by retroviral RNA elements that promote translational readthrough. By modulating the efficiency of translation termination, recognition of long 3′UTRs by Upf1 is uncoupled from the initiation of decay. We propose a model for 3′UTR length surveillance in which equilibrium binding of Upf1 to mRNAs precedes a kinetically distinct commitment to RNA decay.

INTRODUCTION

The nonsense-mediated decay (NMD) machinery executes important regulatory and quality control functions by targeting specific classes of messenger RNAs (mRNAs) for degradation (Chang et al., 2007). In addition to degrading transcripts containing premature termination codons (PTCs) resulting from mutation or rearrangement of genomic DNA or defects in mRNA biogenesis, the pathway is also responsible for regulating between 1% and 10% of all genes in diverse eukaryotes (He et al., 2003; Mendell et al., 2004; Rehwinkel et al., 2005; Wittmann et al., 2006; Weischenfeldt et al., 2008). Transcripts preferentially targeted by NMD include those with PTCs encoded by alternatively spliced exons, introns downstream of the termination codon (TC), long 3′ untranslated regions (3′UTRs), or upstream open reading frames (uORFs; reviewed in Nicholson et al., 2010; Rebbapragada and Lykke-Andersen, 2009). A characteristic that is common to many NMD decay substrates is an extended distance from the terminating ribosome to the mRNA 3′ end (i.e., 3′UTR length). Degradation of aberrant mRNAs by NMD can affect the progression of many human genetic disorders, an estimated one-third of which derive from PTCs (Kuzmiak and Maquat, 2006). In addition, shortening of 3′UTRs has been proposed to relax regulation of mRNA stability and translation, promoting cellular transformation (Sandberg et al., 2008; Wang et al., 2008; Mayr and Bartel, 2009). These findings underscore the importance of understanding the mechanisms by which 3′UTR length is sensed in the process of mRNA quality control.

The well-conserved superfamily I RNA helicase Upf1 is a crucial component of the core NMD machinery. Like other RNA helicases, Upf1 exhibits nonspecific but robust RNA binding activity modulated by ATP binding and hydrolysis (Weng et al., 1998; Bhattacharya et al., 2000). Though the functional roles of Upf1's ATPase and helicase activities are unclear, mutations that abolish its ATPase activity prevent NMD (Weng et al., 1996a, 1996b; Sun et al., 1998). In addition, Upf1 participates in a network of interactions with additional factors proposed to mediate its association with mRNA targets and regulate a cycle of Upf1 phosphorylation and dephosphorylation required for establishment of translational repression and recruitment of RNA decay enzymes (reviewed in Nicholson et al., 2010; see below).

Within the context of a long 3′UTR, additional mRNA features and protein components of mRNPs can promote or inhibit decay. For example, the exon-junction complex (EJC), a multiprotein assembly deposited at exon-exon junctions in the process of splicing, acts through Upf1 to strongly activate decay (Le Hir et al., 2000, 2001; Kim et al., 2001; Lykke-Andersen et al., 2001). The competition between Upf1 and cytoplasmic poly(A)-binding protein 1 (PABPC1) for binding to the translation release factors eRF1 and eRF3 has been proposed to be a crucial factor in the decision to decay diverse transcripts (Ivanov et al., 2008; Singh et al., 2008). Upf1 binding to release factors at the terminating ribosome stimulates phosphorylation of Upf1 by the SMG-1 kinase, translational repression, and recruitment of decay factors (Kashima et al., 2006; Isken et al., 2008; Cho et al., 2009). Conversely, binding of PABPC1 to release factors is proposed to preserve transcript stability and translational competence. In support of this model, artificial tethering approaches and alterations in 3′UTR structure designed to

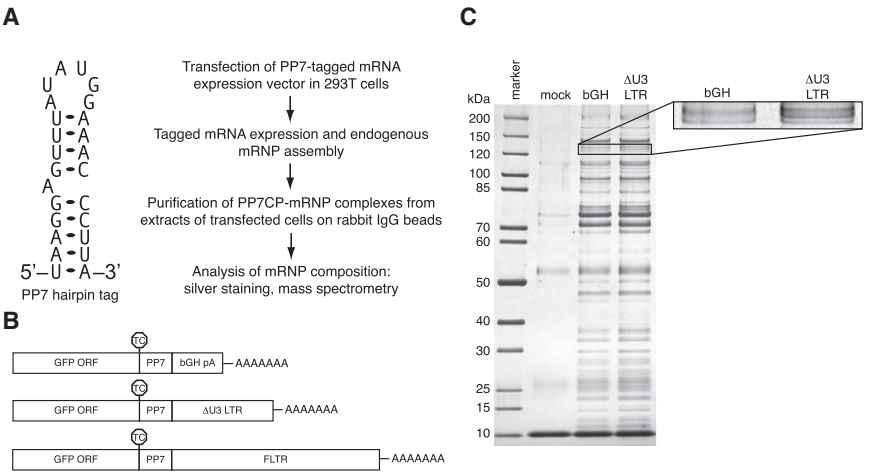

Figure 1. RNA Hairpin-Based Affinity Purification of PP7-Tagged mRNAs

(A) (Left) Predicted secondary structure of the PP7CP RNA-binding site (Lim and Peabody, 2002). (Right) Scheme for purification and analysis of mRNPs containing specific mRNAs.

(B) Tagged mRNAs used for RNA-based affinity purification. RNAs containing the GFP ORF, a single copy of the PP7 RNA hairpin, and the bovine growth hormone polyadenylation element (bGH, top), an HIV 3′LTR variant containing a deletion in the U3 region (ΔU3 LTR, middle), or the full-length HIV 3′LTR (bottom). TC positions are indicated by octagons.

(C) Purification of tagged mRNPs. Proteins copurifying with bGH- or ΔU3 LTR-containing RNAs or present in mock purifications from extracts lacking tagged RNA were separated by SDS-PAGE and detected by silver staining. (Inset) Magnification of the band corresponding to Upf1 (see also Table S1).

mimic 3′UTR shortening by bringing PABPC1 in proximity to the termination codon can suppress Upf1-dependent decay (Amrani et al., 2004; Behm-Ansmant et al., 2007; Eberle et al., 2008; Ivanov et al., 2008; Silva et al., 2008).

Here, we use affinity purification of hairpin-tagged mRNAs to isolate and characterize endogenously assembled mRNP complexes. With this approach, we show that Upf1 assembles into mRNPs in a 3′UTR length-dependent manner. Upf1 copurifies to some extent with all transcripts tested but is highly enriched on mRNAs containing 3′UTRs derived from known NMD targets. The preferential association of Upf1 with mRNAs containing NMD-sensitive 3′UTRs is not affected by inhibition of translation and NMD. Together with our finding that the efficiency of Upf1 coimmunoprecipitation with 3′UTR-derived RNase H cleavage products correlates with fragment length, these observations suggest a direct role for Upf1 in 3′UTR length sensing. To further investigate the in vivo dynamics of 3′UTR length surveillance and decay, we use retroviral elements to induce translational readthrough of NMD-triggering termination codons. Surprisingly, periodic readthrough events can reduce steady-state Upf1 association with transcripts containing long 3′UTRs and robustly inhibit NMD. Moreover, we show that rare readthrough events permit steady-state Upf1 accumulation in mRNPs but prevent initiation of mRNA decay.

Our data inform a model in which equilibrium binding of Upf1 senses 3′UTR length and establishes an RNP state primed for decay. The identification of potential decay targets by Upf1 is coupled to a subsequent commitment to decay, the rate of which is dependent on other aspects of mRNP structure and composition. Furthermore, our data indicate that the decision to decay takes place over a kinetic interval corresponding to many translation termination events. This separation between 3′UTR length sensing and initiation of decay provides a mechanism to prevent aberrant degradation of normal RNAs and presents an opportunity for transcripts to evade cellular mRNA surveillance. Retroviruses may exploit this opportunity by inducing translational readthrough or frameshifting to periodically disrupt the recognition of viral mRNAs as potential decay substrates.

RESULTS

RNA-Based Affinity Purification Identifies Protein Components of Messenger RNPs

To better understand cellular mRNA biogenesis and decay, we have developed a generalizable technique for purification and characterization of endogenously assembled mRNP complexes. In this approach, we singly tag mRNAs with the naturally occurring Pseudomonas phage 7 coat protein (PP7CP) binding site, a 25 nucleotide (nt) stably folding hairpin (Figure 1A; Lim and Peabody, 2002). Tagged RNAs are transiently or stably expressed in appropriate mammalian cell lines, allowing progression through endogenous RNA processing pathways. RNPs assembled on the tagged RNAs are then purified from extracts using a version of the PP7CP tagged with tandem Staphylococcus aureus protein A domains. Previously, a similar method was used to isolate complexes associated with several noncoding RNAs (Hogg and Collins, 2007a, 2007b). In the process of adapting this methodology to the purification of mRNPs, we found that the use of traditional agarose-based resins afforded inefficient purification of tagged mRNP complexes. In contrast, nonporous magnetic resins allowed purification of tagged mRNAs to near homogeneity following a single step of purification (Figures 1A and 1C; additional data not shown).

Recent work in our laboratory has shown that HIV-1 3′LTR sequences play a crucial role in the regulation of viral mRNA biogenesis (Valente and Goff, 2006; Valente et al., 2009). To identify proteins specifically associated with HIV 3′LTR sequences, we constructed a series of PP7-tagged RNAs containing the GFP open reading frame and alternative 3′UTRs (Figure 1B; see below). In our initial experiments, we used a version of the HIV 3′LTR containing a deletion in the U3 region (ΔU3 LTR). The bovine growth hormone polyadenylation (bGH pA) element of the pcDNA3.1 vector was used as a control, aiding discrimination of proteins specifically bound to HIV 3′LTR sequence-containing RNPs. Silver staining of complexes purified from whole-cell extracts of transiently transfected 293T cells revealed that, as expected, each tagged RNA associates with

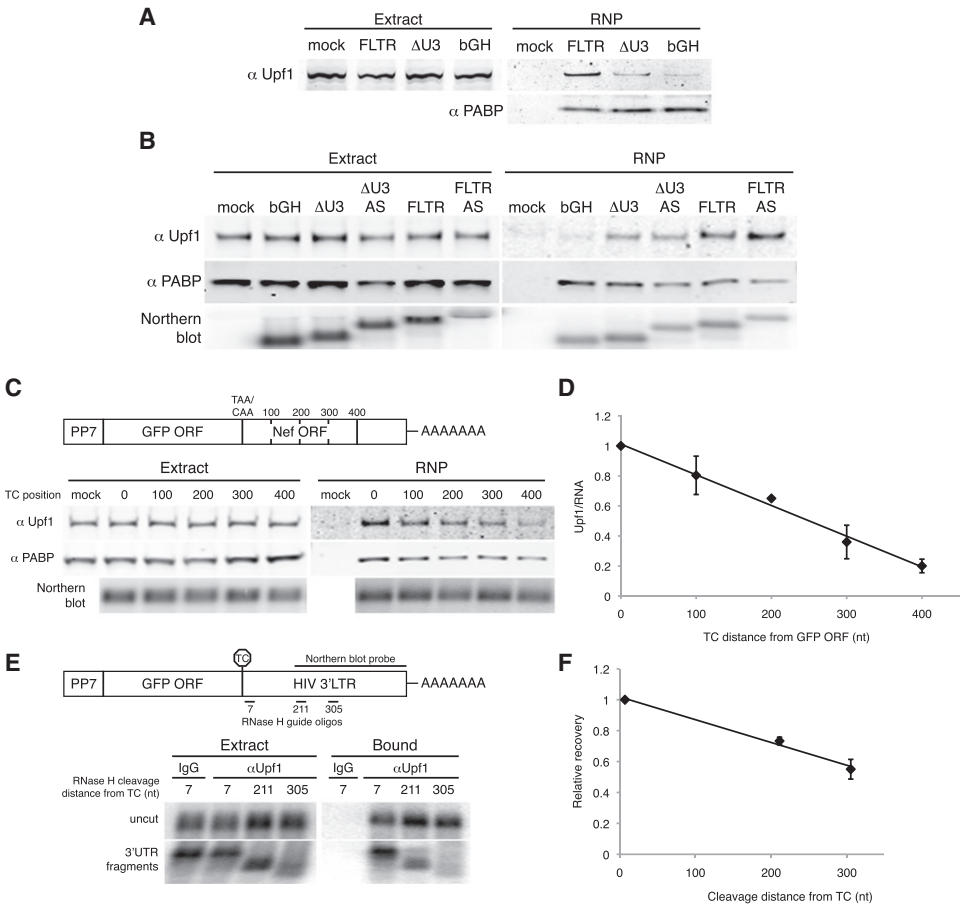

Figure 2. 3′UTR Length-Dependent Interaction of Upf1 with mRNAs

(A) Enrichment of Upf1 on RNAs containing LTR sequence. Proteins in whole-cell extracts of parental 293T cells (mock) or cells transiently transfected with the indicated PP7-tagged RNAs (extract, left) or copurifying with tagged RNAs (RNP, right) were detected by immunoblotting with antibodies against endogenous Upf1 (top) and PABPC1 (bottom).

(B) Sequence-independent assembly of Upf1 in mRNPs. RNPs containing the bGH pA element or full-length or ΔU3 LTRs in the sense (FLTR and ΔU3 LTR) or antisense (ΔU3 AS and FLTR AS) orientations were subjected to purification and immunoblotting as in (A). (Bottom) Small fractions of input extract and purified material were analyzed by northern blotting to detect tagged RNAs.

(C) Upf1 association depends on 3′UTR length. (Top) Constructs encoding RNAs in which the HIV 3′LTR was fused to the GFP ORF, placing the HIV *nef* ORF in frame. RNAs contained the standard GFP TC (0) or a CAA codon in place of the GFP TC in tandem with artificially introduced TCs at 100 nt intervals (100, 200, 300, and 400). (Bottom) RNPs were purified and analyzed by immunoblotting and northern blotting as in (A) and (B).

(D) Quantification of data in (C). Upf1 signal was normalized to RNA signal from northern blotting of a fraction of the purified material and arbitrarily set to 1 for the construct containing the standard GFP TC. Error bars indicate ± SEM; n = 2.

(E) Coimmunoprecipitation of Upf1 with 3′UTR-derived RNase H cleavage products. RNase H cleavage of PP7-GFP-FLTR mRNAs was directed using oligonucleotides hybridizing to FLTR sequences 7, 211, or 305 nt downstream of the GFP TC. Extracts were subjected to immunoprecipitation with an anti-Upf1 antibody or nonspecific IgG, and recovery of uncut mRNAs (top) and 3′UTR fragments (bottom) was monitored by northern blotting using a probe against the indicated portion of the HIV 3′LTR sequence. See also Figure S1A.

(F) Quantification of the data in (E). Recovery of 3′UTR fragments was normalized to the abundance of the fragments in extracts, using the uncut mRNAs as internal controls. The recovery efficiency of the longest 3′UTR fragment (7) was arbitrarily set to 1. Error bars indicate ± SEM; n = 2.

a large number of proteins (Figure 1C and data not shown). Mock purifications from extracts lacking tagged RNAs exhibited very few contaminating proteins, indicating that the vast majority of the proteins visible by silver staining were isolated via their association with tagged mRNPs. Many components of the purified mRNPs are found in all complexes purified, including general translation factors, ribosomes, hnRNP proteins, and other proteins that associate with common mRNA features (Figure 1C and data not shown).

Tandem mass spectrometry of gel slices excised from HIV ΔU3 LTR and bGH copurifying material identified four peptides derived from the Upf1 protein in the ΔU3 LTR sample but none in the bGH control sample (Table S1 available online). Immunoblotting of PP7-purified RNPs confirmed that Upf1 was enriched on transcripts containing HIV 3′LTR sequences, using immunoblotting for PABPC1 as a control for RNP recovery (Figure 2A). We detected Upf1 in association with RNAs containing the bGH pA element, but at much lower levels than those copurifying

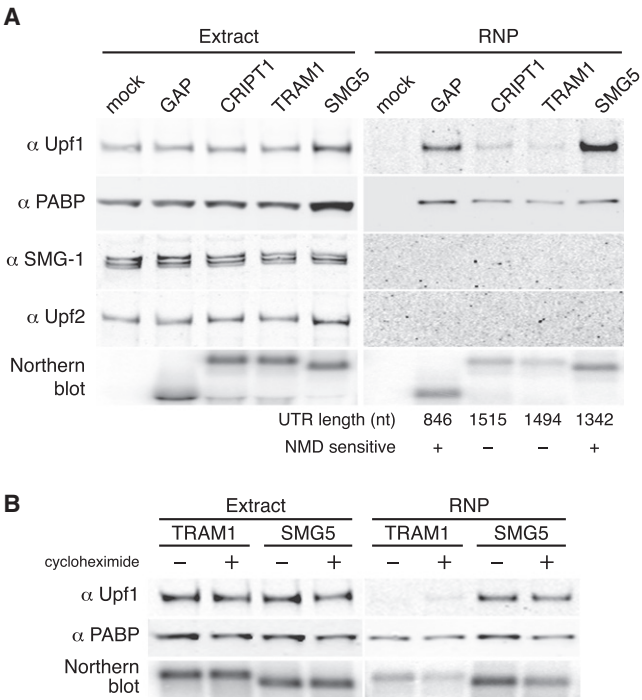

Figure 3. Upf1 Preferentially Associates with Transcripts Containing 3′UTRs Known to Trigger NMD

(A) PP7-tagged GFP mRNAs containing the indicated 3′UTRs were transiently expressed in 293T cells and subjected to affinity purification. Proteins present in whole-cell extracts and purified RNPs were detected by immunoblotting with antibodies against endogenous Upf1, PABPC1, SMG-1, and Upf2. (Bottom) RNA was isolated from small fractions of extracts and purified material and analyzed by northern blotting. See also Figures S1A and S1B.

(B) Upf1 recruitment is insensitive to cycloheximide treatment. 293T cells transiently transfected with PP7-tagged GFP mRNAs containing the TRAM1 or SMG5 3′UTRs were treated (+) or not treated (–) with cycloheximide for 4 hr prior to cell harvest and throughout extract preparation and affinity purification. Immunoblotting and northern blotting were performed as in (A). Inhibition of NMD by cycloheximide and persistence of Upf1 recruitment under conditions of translation inhibition by puromycin and 5′-proximal hairpins are illustrated in Figures S1C–S1F.

with RNAs containing the ΔU3 LTR sequence. Still higher levels of Upf1 were isolated using a full-length LTR (FLTR) comprising intact U3, R, and U5 LTR segments from the pNL4.3 reference HIV genome (Figure 1B and Figure 2A). In agreement with observations of human Upf1 cosedimentation with bulk polysomes and coimmunoprecipitation with diverse mRNAs (Pal et al., 2001; Hosoda et al., 2005), we find that Upf1 associates to some degree with all RNAs tested (Figure 2A, Figure 3A and data not shown). Importantly, we additionally observe substantial transcript-specific enrichment of Upf1 in mRNPs (see below).

Upf1 Associates with Transcripts in a 3′UTR Length-Dependent Manner

To address the specificity of Upf1 association with RNPs containing HIV 3′LTR sequences, we first created tagged RNA constructs in which the ΔU3 or full-length LTR elements were cloned in the antisense orientation, with the bGH pA element provided downstream to ensure proper 3′ end maturation. The requirement for an additional 3′ end-processing element caused the antisense 3′UTRs to be ~200 nt longer than their sense equivalents (Figure 2B, see northern blot). As above, we observed increasing Upf1 copurification with the bGH, ΔU3, and FLTR RNAs, respectively (Figure 2B). Surprisingly, the levels of Upf1 associated with the antisense LTR-containing RNAs were slightly higher than with the corresponding sense 3′UTRs. Thus, the observed recruitment of Upf1 to LTR-containing RNAs was not dependent on primary sequence or structural features. Instead, our data suggested that Upf1 accumulation in mRNPs might be dictated by 3′UTR length.

Current models suggest that 3′UTR length is a crucial determinant of NMD susceptibility (Mühlemann, 2008; Rebbapragada and Lykke-Andersen, 2009), but the mechanism by which 3′UTR length is sensed remains unclear. To test the hypothesis that Upf1 associates with transcripts in a 3′UTR length-dependent manner, we generated a series of 5′ PP7-tagged RNAs consisting of the GFP ORF fused to the HIV FLTR, such that the fragment of the HIV *nef* ORF contained in the LTR was in frame with the GFP ORF (Figure 2C). This series of constructs contains single termination codons at ~100 nt intervals, starting with the original GFP termination codon and ending with the *nef* termination codon ~400 nt downstream. In this way, we varied 3′UTR length by making only one (ablation of the GFP TC) or two (ablation of the GFP TC combined with introduction of a new in-frame TC) point mutations to the RNA primary sequence. Using these constructs, we found that Upf1 copurification with tagged mRNAs increased with 3′UTR length (Figure 2C). The relationship between Upf1 copurification and 3′UTR length was strikingly linear, consistent with sequence-nonspecific recognition of long 3′UTRs by Upf1 (Figure 2D).

Our observations suggested that Upf1 might accomplish 3′UTR length sensing by associating with 3′UTRs. To better understand the basis for 3′UTR length-dependent accumulation of Upf1 in mRNPs, we used RNase H and a series of oligonucleotides directed against HIV 3′LTR sequence to site-specifically cleave 5′-tagged GFP-FLTR mRNAs at sites ~7, ~211, and ~305 nucleotides downstream of the GFP TC. Following RNase H digestion, we immunoprecipitated endogenous Upf1 and assayed mRNA recovery by northern blotting using a probe against HIV 3′LTR sequence. The RNase H cleavage conditions were designed to leave a substantial fraction of the mRNAs intact, allowing the use of full-length mRNAs as recovery controls. FLTR-containing mRNAs were recovered with an antibody against Upf1, but not nonspecific control goat IgG (Figure 2E and Figure S1A). Consistent with our observations above, the efficiency of 3′UTR fragment coimmunoprecipitation increased with RNA length (Figures 2E and 2F). These data suggest that Upf1 association along the length of 3′UTRs accounts for the observed 3′UTR length-dependent accumulation in mRNPs.

Upf1 Preferentially Associates with Transcripts Containing NMD-Sensitive 3′UTRs

Our observation that Upf1 association correlates with 3′UTR length mirrors prior findings that 3′UTR extension causes progressive transcript destabilization in mammalian cells (Bühler et al., 2006; Eberle et al., 2008; Singh et al., 2008). To assess the functional significance of the enrichment of Upf1 on specific

mRNAs, we used a series of long 3′UTRs shown by Singh and colleagues (2008) to either promote or evade decay. As representative NMD-insensitive long 3′UTRs, we used the human CRIPT1 (1515 nt) and TRAM1 (1494 nt) 3′UTRs. To model targets of 3′UTR length-dependent NMD, we used the human SMG5 3′UTR (1342 nt) and an artificial 3′UTR comprising a portion of the GAPDH ORF and the GAPDH 3′UTR (GAP; 846 nt).

As above, we transiently transfected 293T cells with tagged RNA constructs containing model 3′UTRs and isolated mRNPs from whole-cell extracts with PP7CP. Immunoblotting of purified RNPs revealed that Upf1 association strongly correlated with NMD sensitivity (Figure 3A). Very low levels of Upf1 copurified with transcripts containing the NMD-insensitive CRIPT1 and TRAM1 3′UTRs. In contrast, transcripts containing the intronless GAP and SMG5 3′UTRs copurified high levels of Upf1, with the SMG5 3′UTR-containing mRNAs showing the greatest Upf1 recruitment. Likewise, antibodies against Upf1 coimmunoprecipitated mRNAs containing the GAP and SMG5 3′UTRs at higher efficiencies than mRNAs containing the CRIPT and TRAM 3′UTRs (Figure S1A). We did not observe the NMD factors SMG-1 or Upf2 in PP7-purified mRNPs, despite robust detection of the proteins in whole-cell extracts used for purification (Figure 3A). In similar experiments, comparable levels of Upf1 copurified with mRNAs containing the intronless GAP 3′UTR and a version of the GAP 3′UTR containing the adenovirus major-late intron (GAP AdML; Figure S1B). This observation suggests that 3′UTR length is a more significant determinant of Upf1 association than the presence of a spliced intron downstream of the TC. Together, these findings indicate that the extent of Upf1 association with a transcript is diagnostic of its NMD susceptibility, consistent with previous experiments in yeast, *C. elegans*, and human cells (Johansson et al., 2007; Johns et al., 2007; Silva et al., 2008 ; Hwang et al., 2010). In addition, they raise the intriguing possibility that endogenous mRNAs with long 3′UTRs, such as the CRIPT1 and TRAM1 mRNAs, evade NMD by preventing steady-state incorporation of Upf1 into mRNPs.

Preferential Accumulation of Upf1 on Transcripts Containing NMD-Sensitive 3′UTRs Is Independent of Ongoing NMD

We hypothesized that the enrichment of Upf1 on long 3′UTR-containing transcripts could reflect a direct role for the protein in 3′UTR-length sensing prior to the initiation of decay. To address this possibility, we tested the effect of suppressing NMD on Upf1 recruitment by treating cells with the translation elongation inhibitor cycloheximide (Figure 3B). Because initiation of NMD requires translation termination events, cycloheximide potently inhibits NMD (Figure S1C). Following cell growth and extract preparation in cycloheximide, we purified tagged RNAs containing the TRAM1 and SMG5 3′UTRs and analyzed Upf1 association by immunoblotting. Both in the presence and absence of cycloheximide, SMG5 3′UTR-containing RNAs exhibited enhanced copurification of Upf1 relative to TRAM1 3′UTR-containing control RNAs (Figure 3B). Identical results were obtained using the CRIPT1 and GAP 3′UTRs (data not shown). Moreover, the same pattern of Upf1 accumulation in mRNPs was observed upon inhibition of translation elongation with puromycin or translation initiation with a cap-proximal stable hairpin (Figures S1D–S1F). These data demonstrate that Upf1 recruitment is independent of ongoing translation termination and NMD and is therefore well positioned to act as a key determinant of 3′UTR length sensing.

Translational Readthrough Events Reduce Upf1 Association with mRNAs Containing Long 3′UTRs

To probe the in vivo dynamics of 3′UTR length recognition by Upf1, we used retroviral elements to modulate the efficiency of translation termination upstream of an NMD-inducing 3′UTR. Retroviruses control the relative production of Gag and Gag-Pol precursor proteins using RNA motifs that induce regulated readthrough or −1 frameshifting to bypass the *gag* termination codon (Bolinger and Boris-Lawrie, 2009). The Moloney murine leukemia virus pseudoknot (MLVPK), a well-characterized example of the former class, causes misincorporation of an amino acid at the *gag* termination codon with ~4% frequency (Figure S2A) (Wills et al., 1991). Because ribosomes transiting through 3′UTRs are presumably capable of inducing dramatic remodeling of RNP structure, we reasoned that retroviral readthrough-promoting elements might disrupt the recognition of potential NMD substrates.

To determine the effects of translational readthrough on Upf1 accumulation and NMD, we inserted the readthrough-promoting MLVPK sequence in place of the standard GFP termination codon in PP7-tagged RNA constructs, upstream of the artificial GAP 3′UTR. This model NMD-triggering 3′UTR comprises 489 nt of the GAPDH open reading frame and 357 nt of the GAPDH 3′UTR. Readthrough events thus result in termination at the downstream GAPDH TC, a position that does not elicit NMD in reporter transcripts (Figure 4A, top) (Singh et al., 2008; see below). As controls, we inserted an additional termination codon immediately downstream of the MLVPK to prevent readthrough into the GAPDH ORF (MLVPK −C) (Figure 4A, middle) or mutated the upstream termination codon to CAG to allow constitutive translation of the GFP-GAPDH fusion protein (MLVPK CAG) (Figure 4A, bottom). In addition, we used three MLVPK variants with reduced readthrough efficiency to assess the competition between readthrough and Upf1 association: mutation of the wild-type UAG termination codon to UAA (~1.5% readthrough; see Figure S2A for bicistronic dual-luciferase readthrough efficiency assays; Feng et al., 1990), G11C (numbering from termination codon; < 1% readthrough; Felsenstein and Goff, 1992), and A17G (~2% readthrough; Wills et al., 1994).

As expected, immunoblotting of purified RNPs revealed that control mRNAs containing an additional termination codon downstream of the MLVPK efficiently recruited Upf1 (−C) (Figure 4B). In contrast, mRNAs in which the wild-type MLVPK sequence (UAG termination codon) directed intermittent translation of the GAPDH ORF copurified significantly reduced amounts of Upf1. In fact, mRNAs containing the wild-type MLVPK sequence copurified levels of Upf1 similar to those associated with mRNAs lacking an upstream termination codon (CAG) (Figures 4B and 4C). Of interest, the extent of Upf1 association was dependent on the efficiency of readthrough, as the three MLVPK mutants exhibiting reduced readthrough activity copurified high levels of Upf1, similar to the no-readthrough control

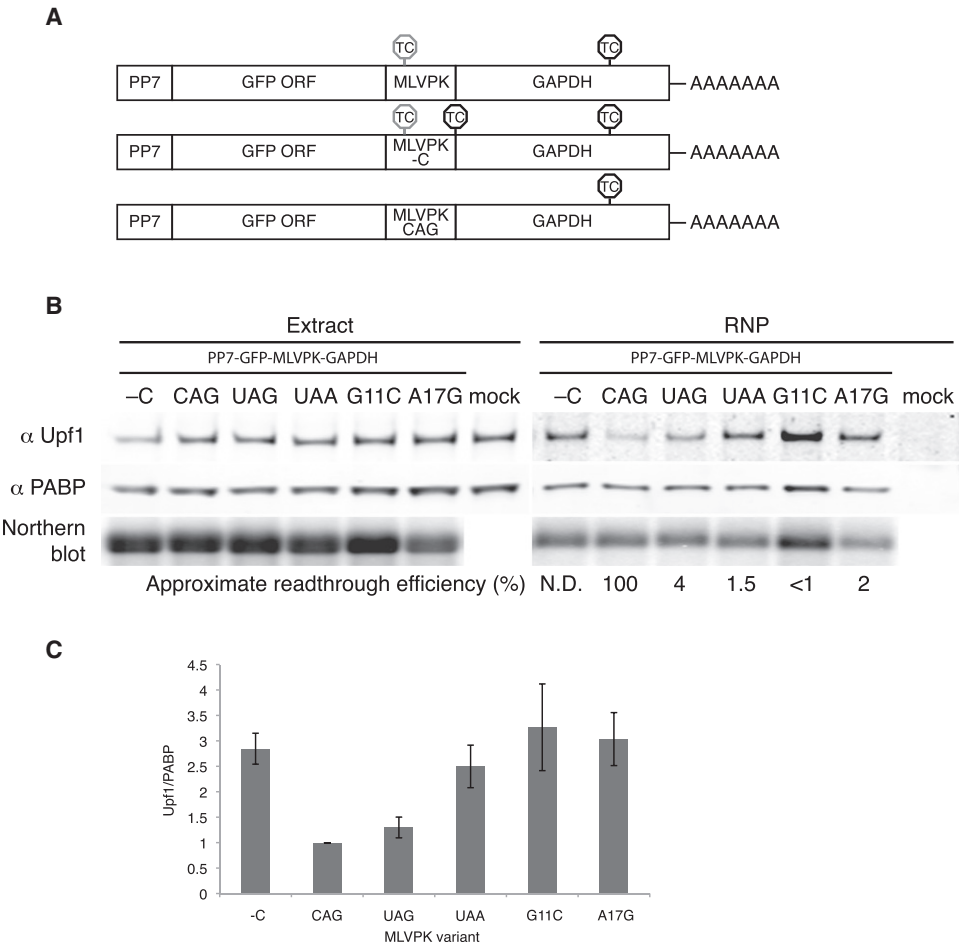

Figure 4. Effects of Translational Readthrough on Upf1 Association

(A) PP7-tagged RNAs containing the GFP ORF in frame with a fragment of the GAPDH ORF were modified to contain the wild-type pseudoknot (top, MLVPK), the MLVPK with an additional in-frame TC downstream (middle, MLVPK –C), or an MLVPK sequence lacking a TC (bottom, MLVPK CAG). Positions of in-frame TCs are indicated. TCs subject to suppression by the MLVPK are indicated by gray octagons; normal TCs are indicated by black octagons.

(B) Tagged mRNAs containing the indicated MLVPK variants were transiently expressed in 293T cells and used for RNA affinity purification. Proteins present in whole-cell extracts and purified material were analyzed by immunoblotting for endogenous Upf1 and PABPC1, and tagged mRNAs were detected by northern blotting. See also Figure S2 for determination of approximate readthrough efficiencies using a bicistronic luciferase assay, disruption of Upf1 binding to mRNAs containing the MMTV −1 frameshifting element, and the effects of puromycin on Upf1 recruitment to MLVPK-containing mRNAs.

(C) Quantification of Upf1 copurification normalized to PABPC1 copurification, arbitrarily set to 1 for the CAG no-TC control. Error bars indicate ± SEM; n = 3.

(Figures 4B and 4C). As a control, we treated cells with puromycin prior to cell extract preparation to confirm that the modulation of Upf1 recruitment by MLVPK was dependent on translation. Indeed, mRNAs containing the wild-type MLVPK and the no-readthrough and constitutive-readthrough controls all copurified similar levels of Upf1 under conditions of puromycin treatment (Figure S2C). In addition, the Mouse mammary tumor virus (MMTV) −1 frameshifting element also inhibited steady-state Upf1 association, demonstrating that the reduction in Upf1 recruitment was independent of the mechanism of termination codon evasion (Figure S2B). These data suggest that the periodic transit of ribosomes through the 3′UTR during readthrough events remodels the mRNP, displacing Upf1. Readthrough events caused by the wild-type MLVPK were sufficiently frequent to repress steady-state Upf1 accumulation, whereas less active MLVPK variants permitted recovery of Upf1 binding to mRNPs. Modulation of readthrough efficiency thus uncovers an equilibrium of Upf1 binding and displacement that marks long 3′UTRs of potential decay targets.

Rare Readthrough Events Protect Transcripts from Decay Independently of Disruption of Steady-State Upf1 Association

The ability of readthrough-promoting elements to reduce steady-state Upf1 association with mRNPs raised the possibility that such elements could also stabilize targets of NMD in mammalian cells. To assess RNA decay, we introduced MLVPK variants into tetracycline (tet)-regulated β-globin reporter RNAs containing the GAP artificial 3′UTR (Figure 5A) (Singh et al., 2008). The indicated tet-regulated constructs were

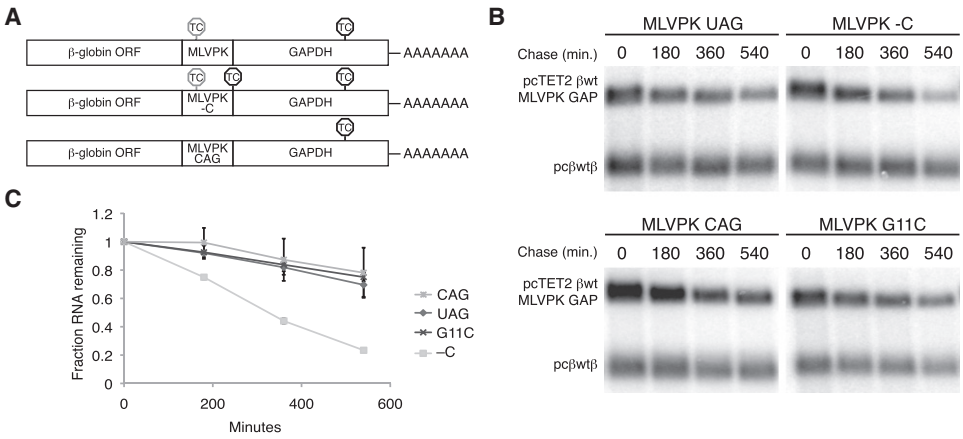

Figure 5. Rare Readthrough Events Stabilize Targets of NMD

(A) Schematic of tet-regulated β-globin reporter mRNA constructs used in RNA decay assays. Constructs contained the β-globin ORF and the GAPDH ORF fragment in frame, with intervening MLVPK sequence to regulate readthrough. Positions of in-frame TCs are indicated. TCs subject to suppression by the MLVPK are indicated by gray octagons; normal TCs are indicated by black octagons.

(B) Decay assays of reporter mRNAs containing MLVPK variants. Constructs encoding the tet-regulated transcripts described in (A) (pcTET2 βwt MLVPK GAP; top bands) were cotransfected with the constitutively expressed wild-type β-globin reporter (pcβwtβ; bottom bands) in HeLa Tet-off cells. RNA was harvested 30 min after transcription was halted by addition of doxycycline and at 3 hr intervals thereafter. See also Figure S3 for decay assays of mRNAs containing the MMTV −1FS element.

(C) Quantification of decay assays. Levels of tet-regulated reporter mRNAs were normalized to levels of the wild-type β-globin transfection control. Error bars indicate ± SEM; n = 3.

cotransfected with CMV promoter-driven β-globin control RNAs into HeLa Tet-off cells. After an interval of transcription induction, we monitored the decay of tet-regulated RNAs for a 9 hr time course by northern blotting (Figures 5B and 5C). As expected, mRNAs lacking an upstream TC (MLVPK CAG) were much more stable than RNAs containing the wild-type MLVPK sequence followed immediately by an additional termination codon (MLVPK –C). Remarkably, all of the MLVPK variants tested, including the minimally active G11C mutant, increased RNA stability to levels indistinguishable from control RNAs lacking an upstream TC (Figures 5B and 5C; additional data not shown). Using the MMTV −1 frameshift element to allow translation of the GAPDH ORF also rescued transcript stability, suggesting that readthrough events stabilize NMD targets independently of the mechanism of translational recoding (Figure S3).

Impaired MLVPK variants allow steady-state Upf1 accumulation in mRNPs but robustly inhibit long 3′UTR-mediated mRNA decay. These findings imply that Upf1 recognition of long 3′UTRs is coupled to a kinetically deferred commitment to decay that is subject to inhibition by rare readthrough events. The presence of an EJC downstream of a TC substantially enhances mRNA decay, potentially by activating Upf1 recruited by long 3′UTRs. We therefore reasoned that the EJC might overcome the effects of readthrough by accelerating the initiation of decay. As a model for EJC-stimulated decay, we used the GAP AdML intron-containing 3′UTR previously shown to direct efficient degradation of reporter transcripts (Singh et al., 2008). Assays of GAP AdML 3′UTR-containing mRNA accumulation revealed that the ability of MLVPK variants to promote RNA stability correlated with readthrough efficiency (Figures 6A and 6B and Figure S4). The wild-type MLVPK sequence permitted mRNA accumulation to levels indistinguishable from those of mRNAs lacking an upstream TC (MLVPK CAG), whereas RNAs containing the mildly impaired UAA and A17G MLVPK variants accumulated to slightly lower levels. The more severe G11C and A39U mutations further reduced RNA accumulation but nevertheless allowed ~4-fold higher RNA levels than the no-readthrough control (MLVPK −C). Decay assay time courses confirmed that the MLVPK-containing RNAs were indeed stabilized relative to the no-readthrough control transcripts (Figure S4). These data show that even efficient EJC-stimulated NMD can be significantly impaired by instances of readthrough occurring at less than 1% of all possible termination events. In addition, the differential stability of transcripts undergoing readthrough of varying efficiency points to the existence of a rate-limiting step downstream of Upf1 association that can be accelerated by the EJC (see Discussion).

DISCUSSION

The identification of proteins copurifying with PP7-tagged RNAs by mass spectrometry allows unbiased analysis of the effects of RNA sequence, structure, and biogenesis pathway on mRNP composition. Using this system, we show that the extent of Upf1 association with specific transcripts strongly correlates with NMD susceptibility, as Upf1 is highly enriched on transcripts containing 3′UTRs derived from known NMD targets. Analysis of mRNPs containing HIV 3′LTR-derived and other model 3′UTR sequences revealed that Upf1 recruitment increases with 3′UTR length but is independent of ongoing translation and NMD. Moreover, we show that Upf1 coimmunoprecipitates 3′UTR-derived RNase H cleavage products in a fragment length-dependent manner, suggesting that Upf1 is associated along the length of 3′UTRs. The enrichment of Upf1 on long

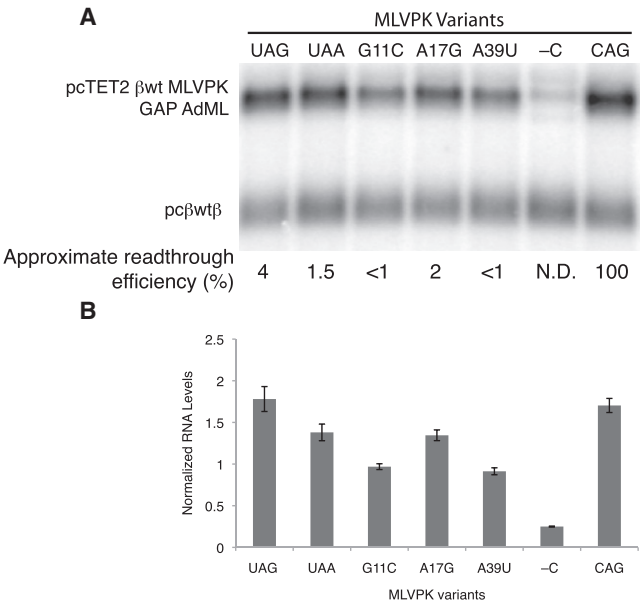

Figure 6. Readthrough Inhibits EJC-Stimulated NMD

(A) Northern blot of RNA accumulation in HeLa Tet-off cells cotransfected with constitutively expressed wild-type β-globin transcripts (pcβwtβ; bottom bands) and tet-regulated β-globin transcripts containing the GAP AdML 3′UTR and the indicated MLVPK variants (pcTET2 βwt MLVPK GAP AdML; top bands). See Figure S4 for decay assays.

(B) Quantification of RNA accumulation assays. Levels of tet-regulated reporter RNAs were normalized to levels of the wild-type β-globin transfection control. Error bars indicate ± SEM; n = 3.

3′UTR-containing transcripts may increase the probability that Upf1 will outcompete PABPC1 for release factor binding and trigger NMD, providing a potential mechanism for the correlation between 3′UTR length and transcript stability in human cells (Bühler et al., 2006; Eberle et al., 2008; Singh et al., 2008).

With the expectation that readthrough events would cause elongating ribosomes to periodically strip Upf1 and other proteins from the mRNA downstream of the bypassed termination codon, we modulated readthrough efficiency to probe the dynamics of Upf1 association. We show that the activity of wild-type MLVPK, which causes ~4% readthrough, suppresses steady-state Upf1 recruitment to the artificial GAP 3′UTR. Less frequent readthrough events, in contrast, allow complete recovery of Upf1 binding to mRNPs. Together, our observations suggest that Upf1 accumulation on transcripts is not simply dependent on the site of the vast majority of termination events but is instead determined by sequence-nonspecific association of Upf1 with 3′UTRs. Differential disruption of Upf1 binding by readthrough events of varying efficiency therefore reveals an equilibrium of Upf1 association that can serve as a mechanism for sensing 3′UTR length.

Equilibrium binding of Upf1 to mRNPs may be influenced by several factors, including Upf1 RNA binding affinity, interactions with additional mRNP components, and disruption by elongating ribosomes. The ATP binding and hydrolysis cycle of Upf1 modulates the protein's sequence-nonspecific RNA binding activity, providing a potential mechanism to regulate Upf1 association with mRNPs (Weng et al., 1998; Bhattacharya et al., 2000). It is possible that Upf1 recruitment to long 3′UTRs is mediated by protein-protein interactions, but scrutiny of silver-stained gels of purified RNPs and immunoblotting for known NMD factors did not reveal additional proteins that showed patterns of copurification similar to Upf1 (1C, Figure 3A, and data not shown). In addition, Upf1 association was maintained despite treatment with EDTA and inhibition of translation by multiple means, indicating that an interaction with intact ribosomes is not responsible for the observed accumulation of Upf1 in mRNPs (Figure 3B and Figures S1C–S1G).

Based on our findings that rare readthrough events permit Upf1 3′UTR length-dependent accumulation in mRNPs but inhibit decay, we propose a two-step model in which Upf1 senses 3′UTR length to potentiate decay (Figure 7). In this model, length-dependent equilibrium binding of Upf1 marks 3′UTRs of potential decay substrates and increases the probability of Upf1 binding to release factors. Upf1 accumulation in mRNPs is necessary, but not sufficient, to initiate mRNA degradation and is instead followed by a kinetically distinct commitment to decay. The decision to decay is determined by the activity of Upf1 and additional mRNP factors, including the EJC and PABPC1. Here, we provide evidence that 3′UTR recognition and decay commitment steps can be separated by modulating readthrough efficiency: frequent readthrough events disrupt 3′UTR length sensing by displacing Upf1 from 3′UTR sequence, and rare readthrough events allow Upf1 association but prevent one or more rate-limiting steps required for initiation of decay. Potential rate-limiting steps subject to disruption by infrequent translational readthrough include ATP binding and hydrolysis by Upf1, the formation of the Upf (Upf1-Upf2-Upf3b) or SURF (SMG-1-Upf1-eRF1-eRF3) complexes, Upf1 phosphorylation, and the recruitment and/or activity of the RNA degradation machinery. We find that the presence of a spliced intron downstream of the TC partially restores decay in the context of rare readthrough events, indicating that one key event may be stimulated by the EJC, such as Upf1 ATPase activity or phosphorylation (Kashima et al., 2006; Wittmann et al., 2006; Chamieh et al., 2008).

An important consequence of the delay between length-dependent Upf1 accumulation in mRNPs and initiation of decay may be improved quality control fidelity. Based on a release factor-dependent nonsense error rate of 1 in 10^5 codons (Jørgensen et al., 1993), aberrant termination events are predicted to occur on ~50% of transcripts encoding 50 kDa proteins during the course of 100 translation events. Integrating the decision to decay over several termination events provides a mechanism to avoid degradation in response to translational errors while preserving the ability to recognize DNA- or RNA-encoded PTCs. This mechanism may also prevent immediate decay upon binding of Upf1 to release factors at a normal TC, which may occur at a significant frequency as suggested by studies of Upf1 and PABP release factor association (Ivanov et al., 2008; Singh et al., 2008).

In mammals, NMD has been proposed to exclusively target newly exported mRNA during a pioneer round or rounds of translation that are biochemically distinguished by the presence of the nuclear cap-binding proteins CBP80/20 in the mRNP (Maquat

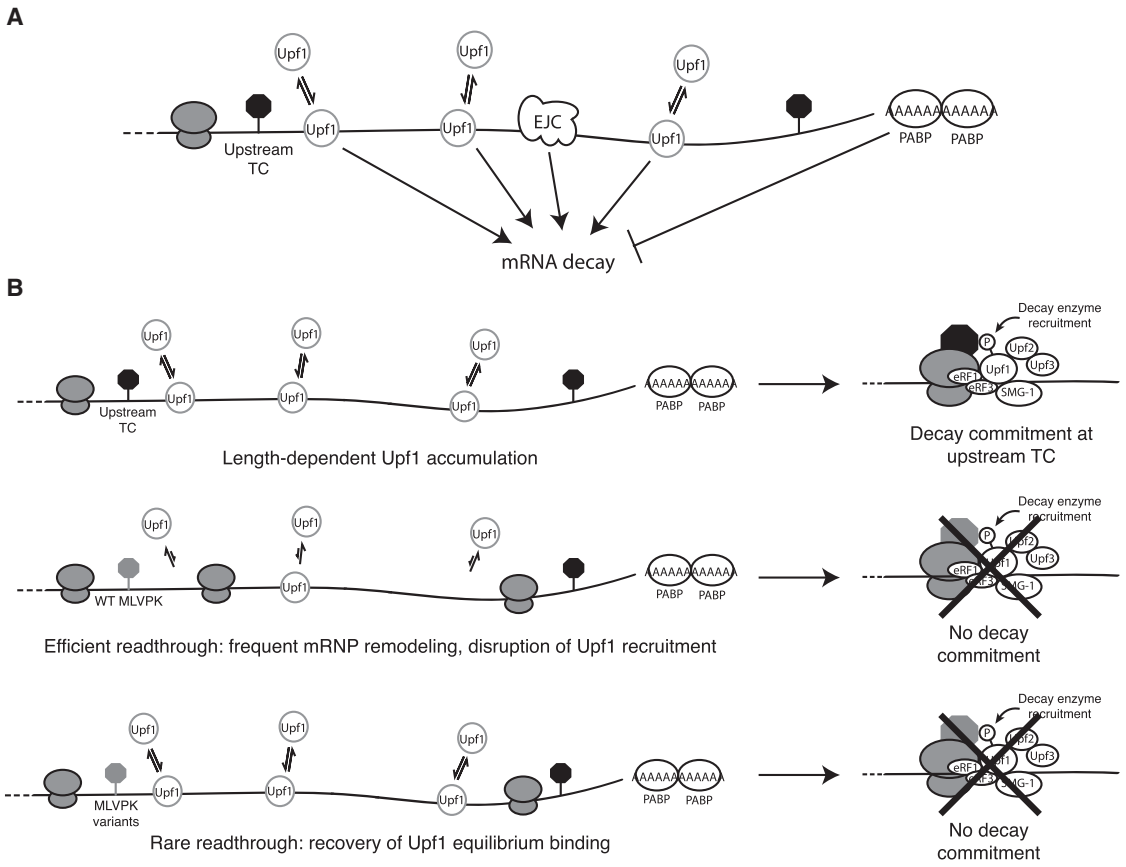

Figure 7. Model for 3′UTR Length Surveillance by Upf1

(A) Equilibrium length-dependent binding of Upf1 marks long 3′UTRs as potential decay targets. Other aspects of RNP structure and composition, such as the EJC and PABPC1, can stimulate or repress decay potentiated by Upf1 association.

(B) Inhibition of Upf1-dependent decay by translational readthrough. (Top) 3′UTR length-dependent accumulation of Upf1 increases the likelihood of Upf1 binding to release factors and precedes the initiation of decay. (Middle) Readthrough induced by the wild-type MLVPK disrupts steady-state accumulation of Upf1 on mRNAs containing long 3′UTRs and inhibits decay. (Bottom) MLVPK variants causing low levels of readthrough allow recovery of Upf1 equilibrium binding but inhibit a kinetically distinct decay commitment step. Candidate rate-limiting steps required for decay initiation are discussed in the main text.

et al., 2010). Replacement of CBP80/20 with translation initiation factor eIF4E marks entry of an mRNP into bulk translation and is thought to confer resistance to NMD. We observe substantial stabilization of transcripts containing elements that direct readthrough at less than 1% efficiency, suggesting that the decision to decay spans an interval corresponding to many translation termination events. These findings mirror the effects of altering termination efficiency in yeast, in which NMD surveillance is conducted throughout the lifetime of a transcript (Zhang et al., 1997; Maderazo et al., 2003; Keeling et al., 2004). The ability of rare readthrough events to inhibit NMD in mammalian cells is supported by multiple reports of readthrough-promoting drugs or inefficient selenocysteine incorporation at UGA codons inducing accumulation of decay targets (Bedwell et al., 1997; Moriarty et al., 1998; Weiss and Sunde, 1998; Mehta et al., 2004; Allamand et al., 2008; Salvatori et al., 2009). Therefore, we hypothesize that mammalian NMD is able to degrade mRNAs that have proceeded beyond the pioneer round(s) of translation.

EXPERIMENTAL PROCEDURES

Constructs

For details of plasmid construction, see Extended Experimental Procedures.

Cell Culture and Extracts

293T cells were maintained, transfected, and used for cell extract preparation essentially as described (Hogg and Collins, 2007b). For details, see Extended Experimental Procedures.

RNA-Based Affinity Purification of mRNPs and Immunoprecipitation

All mRNP purification steps were performed at 4°C. Whole-cell extracts prepared in 20 mM HEPES (pH 7.6), 150 mM NaCl, 2 mM $MgCl_2$, 10% glycerol, 1 mM DTT, and protease inhibitors (HLB150) were supplemented with 0.1% NP-40 and ~1 ug/ml ZZ-tev-PP7CP expressed and purified in *E. coli* as described (Hogg and Collins, 2007b). After rotating for 60 min, 4.5 mg of M-270 epoxy Dynabeads (Invitrogen) conjugated with rabbit IgG (Oeffinger et al., 2007) were added per ml of extract, followed by an additional 60 min incubation. Beads were collected using a magnetic particle concentrator (Invitrogen) and extensively washed in HLB150 + 0.1% NP-40. RNP proteins were eluted from beads using LDS buffer (Invitrogen) for immunoblotting or 1:50 diluted RNase A/T1 mix (Ambion) in 100 mM ammonium bicarbonate for silver

staining and mass spectrometry. For details of mass spectrometry and RNase H cleavage and immunoprecipitation experiments, see Extended Experimental Procedures.

RNA Decay and Accumulation Assays

RNA decay assays were performed as described, with modifications (Singh et al., 2008). For details, see Extended Experimental Procedures.

Detection of RNA and Protein

Northern blots were imaged on a Typhoon Trio and quantified using ImageQuant software (G.E.). Immunoblots were imaged and quantified on the Odyssey Infrared Imaging System (LI-COR). For information on probes and antibodies used, see Extended Experimental Procedures.

SUPPLEMENTAL INFORMATION

Supplemental Information includes Extended Experimental Procedures, four figures, and one table and can be found with this article online at doi: 10.1016/j.cell.2010.10.005.

ACKNOWLEDGMENTS

We thank Jens Lykke-Andersen and Brian Houck-Loomis for generously providing reagents and Kathleen Collins, Lisa Postow, and Jason Rodriguez for critical reading of the manuscript. Mass spectrometry was performed by Mary Ann Gawinowicz in the Columbia University Medical Center protein core facility. J.R.H. is supported by NRSA postdoctoral fellowship 1F32GM087737. S.P.G. is an investigator of the Howard Hughes Medical Institute.

Received: April 16, 2010
Revised: August 3, 2010
Accepted: October 1, 2010
Published: October 28, 2010

REFERENCES

Allamand, V., Bidou, L., Arakawa, M., Floquet, C., Shiozuka, M., Paturneau-Jouas, M., Gartioux, C., Butler-Browne, G.S., Mouly, V., Rousset, J.-P., et al. (2008). Drug-induced readthrough of premature stop codons leads to the stabilization of laminin α2 chain mRNA in CMD myotubes. J. Gene Med. *10*, 217–224.

Amrani, N., Ganesan, R., Kervestin, S., Mangus, D.A., Ghosh, S., and Jacobson, A. (2004). A *faux* 3′-UTR promotes aberrant termination and triggers nonsense-mediated mRNA decay. Nature *432*, 112–118.

Bedwell, D.M., Kaenjak, A., Benos, D.J., Bebok, Z., Bubien, J.K., Hong, J., Tousson, A., Clancy, J.P., and Sorscher, E.J. (1997). Suppression of a CFTR premature stop mutation in a bronchial epithelial cell line. Nat. Med. *3*, 1280–1284.

Behm-Ansmant, I., Gatfield, D., Rehwinkel, J., Hilgers, V., and Izaurralde, E. (2007). A conserved role for cytoplasmic poly(A)-binding protein 1 (PABPC1) in nonsense-mediated mRNA decay. EMBO J. *26*, 1591–1601.

Bhattacharya, A., Czaplinski, K., Trifillis, P., He, F., Jacobson, A., and Peltz, S.W. (2000). Characterization of the biochemical properties of the human Upf1 gene product that is involved in nonsense-mediated mRNA decay. RNA *6*, 1226–1235.

Bolinger, C., and Boris-Lawrie, K. (2009). Mechanisms employed by retroviruses to exploit host factors for translational control of a complicated proteome. Retrovirology *6*, 8.

Bühler, M., Steiner, S., Mohn, F., Paillusson, A., and Mühlemann, O. (2006). EJC-independent degradation of nonsense immunoglobulin-μ mRNA depends on 3′ UTR length. Nat. Struct. Mol. Biol. *13*, 462–464.

Chamieh, H., Ballut, L., Bonneau, F., and Le Hir, H. (2008). NMD factors UPF2 and UPF3 bridge UPF1 to the exon junction complex and stimulate its RNA helicase activity. Nat. Struct. Mol. Biol. *15*, 85–93.

Chang, Y.-F., Imam, J.S., and Wilkinson, M.F. (2007). The nonsense-mediated decay RNA surveillance pathway. Annu. Rev. Biochem. *76*, 51–74.

Cho, H., Kim, K.M., and Kim, Y.K. (2009). Human proline-rich nuclear receptor coregulatory protein 2 mediates an interaction between mRNA surveillance machinery and decapping complex. Mol. Cell *33*, 75–86.

Eberle, A.B., Stalder, L., Mathys, H., Orozco, R.Z., and Mühlemann, O. (2008). Posttranscriptional gene regulation by spatial rearrangement of the 3′ untranslated region. PLoS Biol. *6*, e92.

Felsenstein, K.M., and Goff, S.P. (1992). Mutational analysis of the gag-pol junction of Moloney murine leukemia virus: requirements for expression of the gag-pol fusion protein. J. Virol. *66*, 6601–6608.

Feng, Y.X., Copeland, T.D., Oroszlan, S., Rein, A., and Levin, J.G. (1990). Identification of amino acids inserted during suppression of UAA and UGA termination codons at the gag-pol junction of Moloney murine leukemia virus. Proc. Natl. Acad. Sci. USA *87*, 8860–8863.

He, F., Li, X., Spatrick, P., Casillo, R., Dong, S., and Jacobson, A. (2003). Genome-wide analysis of mRNAs regulated by the nonsense-mediated and 5′ to 3′ mRNA decay pathways in yeast. Mol. Cell *12*, 1439–1452.

Hogg, J.R., and Collins, K. (2007a). Human Y5 RNA specializes a Ro ribonucleoprotein for 5S ribosomal RNA quality control. Genes Dev. *21*, 3067–3072.

Hogg, J.R., and Collins, K. (2007b). RNA-based affinity purification reveals 7SK RNPs with distinct composition and regulation. RNA *13*, 868–880.

Hosoda, N., Kim, Y.K., Lejeune, F., and Maquat, L.E. (2005). CBP80 promotes interaction of Upf1 with Upf2 during nonsense-mediated mRNA decay in mammalian cells. Nat. Struct. Mol. Biol. *12*, 893–901.

Hwang, J., Sato, H., Tang, Y., Matsuda, D., and Maquat, L.E. (2010). UPF1 association with the cap-binding protein, CBP80, promotes nonsense-mediated mRNA decay at two distinct steps. Mol. Cell *39*, 396–409.

Isken, O., Kim, Y.K., Hosoda, N., Mayeur, G.L., Hershey, J.W.B., and Maquat, L.E. (2008). Upf1 phosphorylation triggers translational repression during nonsense-mediated mRNA decay. Cell *133*, 314–327.

Ivanov, P.V., Gehring, N.H., Kunz, J.B., Hentze, M.W., and Kulozik, A.E. (2008). Interactions between UPF1, eRFs, PABP and the exon junction complex suggest an integrated model for mammalian NMD pathways. EMBO J. *27*, 736–747.

Johansson, M.J.O., He, F., Spatrick, P., Li, C., and Jacobson, A. (2007). Association of yeast Upf1p with direct substrates of the NMD pathway. Proc. Natl. Acad. Sci. USA *104*, 20872–20877.

Johns, L., Grimson, A., Kuchma, S.L., Newman, C.L., and Anderson, P. (2007). *Caenorhabditis elegans* SMG-2 selectively marks mRNAs containing premature translation termination codons. Mol. Cell. Biol. *27*, 5630–5638.

Jørgensen, F., Adamski, F.M., Tate, W.P., and Kurland, C.G. (1993). Release factor-dependent false stops are infrequent in Escherichia coli. J. Mol. Biol. *230*, 41–50.

Kashima, I., Yamashita, A., Izumi, N., Kataoka, N., Morishita, R., Hoshino, S., Ohno, M., Dreyfuss, G., and Ohno, S. (2006). Binding of a novel SMG-1-Upf1-eRF1-eRF3 complex (SURF) to the exon junction complex triggers Upf1 phosphorylation and nonsense-mediated mRNA decay. Genes Dev. *20*, 355–367.

Keeling, K.M., Lanier, J., Du, M., Salas-Marco, J., Gao, L., Kaenjak-Angeletti, A., and Bedwell, D.M. (2004). Leaky termination at premature stop codons antagonizes nonsense-mediated mRNA decay in S. cerevisiae. RNA *10*, 691–703.

Kim, V.N., Kataoka, N., and Dreyfuss, G. (2001). Role of the nonsense-mediated decay factor hUpf3 in the splicing-dependent exon-exon junction complex. Science *293*, 1832–1836.

Kuzmiak, H.A., and Maquat, L.E. (2006). Applying nonsense-mediated mRNA decay research to the clinic: progress and challenges. Trends Mol. Med. *12*, 306–316.

Le Hir, H., Gatfield, D., Izaurralde, E., and Moore, M.J. (2001). The exon-exon junction complex provides a binding platform for factors involved in mRNA export and nonsense-mediated mRNA decay. EMBO J. *20*, 4987–4997.

Le Hir, H., Izaurralde, E., Maquat, L.E., and Moore, M.J. (2000). The spliceosome deposits multiple proteins 20-24 nucleotides upstream of mRNA exon-exon junctions. EMBO J. *19*, 6860–6869.

Lim, F., and Peabody, D.S. (2002). RNA recognition site of PP7 coat protein. Nucleic Acids Res. *30*, 4138–4144.

Lykke-Andersen, J., Shu, M.D., and Steitz, J.A. (2001). Communication of the position of exon-exon junctions to the mRNA surveillance machinery by the protein RNPS1. Science *293*, 1836–1839.

Maderazo, A.B., Belk, J.P., He, F., and Jacobson, A. (2003). Nonsense-containing mRNAs that accumulate in the absence of a functional nonsense-mediated mRNA decay pathway are destabilized rapidly upon its restitution. Mol. Cell. Biol. *23*, 842–851.

Maquat, L.E., Tarn, W.Y., and Isken, O. (2010). The pioneer round of translation: features and functions. Cell *142*, 368–374.

Mayr, C., and Bartel, D.P. (2009). Widespread shortening of 3'UTRs by alternative cleavage and polyadenylation activates oncogenes in cancer cells. Cell *138*, 673–684.

Mehta, A., Rebsch, C.M., Kinzy, S.A., Fletcher, J.E., and Copeland, P.R. (2004). Efficiency of mammalian selenocysteine incorporation. J. Biol. Chem. *279*, 37852–37859.

Mendell, J.T., Sharifi, N.A., Meyers, J.L., Martinez-Murillo, F., and Dietz, H.C. (2004). Nonsense surveillance regulates expression of diverse classes of mammalian transcripts and mutes genomic noise. Nat. Genet. *36*, 1073–1078.

Moriarty, P.M., Reddy, C.C., and Maquat, L.E. (1998). Selenium deficiency reduces the abundance of mRNA for Se-dependent glutathione peroxidase 1 by a UGA-dependent mechanism likely to be nonsense codon-mediated decay of cytoplasmic mRNA. Mol. Cell. Biol. *18*, 2932–2939.

Mühlemann, O. (2008). Recognition of nonsense mRNA: towards a unified model. Biochem. Soc. Trans. *36*, 497–501.

Nicholson, P., Yepiskoposyan, H., Metze, S., Zamudio Orozco, R., Kleinschmidt, N., and Mühlemann, O. (2010). Nonsense-mediated mRNA decay in human cells: mechanistic insights, functions beyond quality control and the double-life of NMD factors. Cell. Mol. Life Sci. *67*, 677–700.

Oeffinger, M., Wei, K.E., Rogers, R., DeGrasse, J.A., Chait, B.T., Aitchison, J.D., and Rout, M.P. (2007). Comprehensive analysis of diverse ribonucleoprotein complexes. Nat. Methods *4*, 951–956.

Pal, M., Ishigaki, Y., Nagy, E., and Maquat, L.E. (2001). Evidence that phosphorylation of human Upfl protein varies with intracellular location and is mediated by a wortmannin-sensitive and rapamycin-sensitive PI 3-kinase-related kinase signaling pathway. RNA *7*, 5–15.

Rebbapragada, I., and Lykke-Andersen, J. (2009). Execution of nonsense-mediated mRNA decay: what defines a substrate? Curr. Opin. Cell Biol. *21*, 394–402.

Rehwinkel, J., Letunic, I., Raes, J., Bork, P., and Izaurralde, E. (2005). Nonsense-mediated mRNA decay factors act in concert to regulate common mRNA targets. RNA *11*, 1530–1544.

Salvatori, F., Breveglieri, G., Zuccato, C., Finotti, A., Bianchi, N., Borgatti, M., Feriotto, G., Destro, F., Canella, A., Brognara, E., et al. (2009). Production of β-globin and adult hemoglobin following G418 treatment of erythroid precursor cells from homozygous $\beta^0$39 thalassemia patients. Am. J. Hematol. *84*, 720–728.

Sandberg, R., Neilson, J.R., Sarma, A., Sharp, P.A., and Burge, C.B. (2008). Proliferating cells express mRNAs with shortened 3′ untranslated regions and fewer microRNA target sites. Science *320*, 1643–1647.

Silva, A.L., Ribeiro, P., Inácio, A., Liebhaber, S.A., and Romão, L. (2008). Proximity of the poly(A)-binding protein to a premature termination codon inhibits mammalian nonsense-mediated mRNA decay. RNA *14*, 563–576.

Singh, G., Rebbapragada, I., and Lykke-Andersen, J. (2008). A competition between stimulators and antagonists of Upf complex recruitment governs human nonsense-mediated mRNA decay. PLoS Biol. *6*, e111.

Sun, X., Perlick, H.A., Dietz, H.C., and Maquat, L.E. (1998). A mutated human homologue to yeast Upf1 protein has a dominant-negative effect on the decay of nonsense-containing mRNAs in mammalian cells. Proc. Natl. Acad. Sci. USA *95*, 10009–10014.

Valente, S.T., Gilmartin, G.M., Mott, C., Falkard, B., and Goff, S.P. (2009). Inhibition of HIV-1 replication by eIF3f. Proc. Natl. Acad. Sci. USA *106*, 4071–4078.

Valente, S.T., and Goff, S.P. (2006). Inhibition of HIV-1 gene expression by a fragment of hnRNP U. Mol. Cell *23*, 597–605.

Wang, E.T., Sandberg, R., Luo, S., Khrebtukova, I., Zhang, L., Mayr, C., Kingsmore, S.F., Schroth, G.P., and Burge, C.B. (2008). Alternative isoform regulation in human tissue transcriptomes. Nature *456*, 470–476.

Weischenfeldt, J., Damgaard, I., Bryder, D., Theilgaard-Mönch, K., Thoren, L.A., Nielsen, F.C., Jacobsen, S.E.W., Nerlov, C., and Porse, B.T. (2008). NMD is essential for hematopoietic stem and progenitor cells and for eliminating by-products of programmed DNA rearrangements. Genes Dev. *22*, 1381–1396.

Weiss, S.L., and Sunde, R.A. (1998). Cis-acting elements are required for selenium regulation of glutathione peroxidase-1 mRNA levels. RNA *4*, 816–827.

Weng, Y., Czaplinski, K., and Peltz, S.W. (1996a). Genetic and biochemical characterization of mutations in the ATPase and helicase regions of the Upf1 protein. Mol. Cell. Biol. *16*, 5477–5490.

Weng, Y., Czaplinski, K., and Peltz, S.W. (1996b). Identification and characterization of mutations in the UPF1 gene that affect nonsense suppression and the formation of the Upf protein complex but not mRNA turnover. Mol. Cell. Biol. *16*, 5491–5506.

Weng, Y., Czaplinski, K., and Peltz, S.W. (1998). ATP is a cofactor of the Upf1 protein that modulates its translation termination and RNA binding activities. RNA *4*, 205–214.

Wills, N.M., Gesteland, R.F., and Atkins, J.F. (1991). Evidence that a downstream pseudoknot is required for translational read-through of the Moloney murine leukemia virus gag stop codon. Proc. Natl. Acad. Sci. USA *88*, 6991–6995.

Wills, N.M., Gesteland, R.F., and Atkins, J.F. (1994). Pseudoknot-dependent read-through of retroviral gag termination codons: importance of sequences in the spacer and loop 2. EMBO J. *13*, 4137–4144.

Wittmann, J., Hol, E.M., and Jäck, H.-M. (2006). hUPF2 silencing identifies physiologic substrates of mammalian nonsense-mediated mRNA decay. Mol. Cell. Biol. *26*, 1272–1287.

Zhang, S., Welch, E.M., Hogan, K., Brown, A.H., Peltz, S.W., and Jacobson, A. (1997). Polysome-associated mRNAs are substrates for the nonsense-mediated mRNA decay pathway in *Saccharomyces cerevisiae*. RNA *3*, 234–244.

EXTENDED EXPERIMENTAL PROCEDURES

Plasmid Construction

All plasmid sequences are available upon request. RNA tags were cloned as described (Hogg and Collins, 2007b) and consisted of single tobramycin aptamer and PP7 hairpins cloned between the NheI and HindIII (5′-tagged constructs; pcDNATPGFP) or XbaI and ApaI (3′-tagged constructs; pcDNAGFPTP) sites of pcDNA3.1 (Invitrogen). For pcDNAGFPTPΔU3LTR and pcDNAGFPTPFLTR constructs, the bGH pA element of pcDNA3.1 containing the tag cassette between the NheI and HindIII sites was ablated by digestion with PmeI and DraIII, overhang filling with Klenow fragment, and religation. The ΔU3 LTR and FLTR sequences were amplified by PCR from Trip-TK and HIV-neo plasmids (Valente and Goff, 2006), respectively, and inserted between the KpnI and XbaI sites of the resulting vector. The GFP ORF was inserted into the NheI site (pcDNAGFPTPΔU3LTR and pcDNAGFPTPFLTR constructs) or between the HindIII and XbaI sites (all other tagged RNA constructs) of pcDNA3.1. FLTR-containing plasmids used in Figure 2C were constructed by amplifying and cloning the fragment of pcDNAGFPTPFLTR bounded by XbaI and PstI sites by Sequence and Ligation Independent Cloning (SLIC; (Li and Elledge, 2007) into the corresponding sites of pcDNATPGFP. The TAA TC of GFP was either left intact or mutated to CAA, allowing translation through the in-frame partial *nef* ORF. Additional TCs were introduced by site-directed mutagenesis. To create pcDNAGFPTPΔU3LTRAS and pcDNAGFPTPFLTRAS, the LTR sequences were amplified as above and cloned in the reverse orientation into the ApaI site of pcDNAGFPTP, upstream of the bGH pA element to ensure proper 3′ end formation. The GAP, GAP AdML, CRIPT, TRAM, and SMG5 3′UTRs were amplified from plasmids provided by Jens Lykke-Andersen and cloned into the ApaI site of pcDNAGFPTP (Singh et al., 2008). To inhibit translation initiation, stable hairpin HP40 (Babendure et al., 2006) was inserted by SLIC between the SacI and NheI sites of the indicated vectors, such that the hairpin structure began at the first nucleotide following the pcDNA3.1 transcriptional start site. MLVPK and MMTV −1FS elements were inserted into the XbaI site of the pcDNATPGFP vector by SLIC using overlapping oligos designed to replace the GFP TC with a CAA codon. The GAP 3′UTR was inserted into the ApaI site of the resulting vectors, in frame with the GFP ORF (MLVPK) or in the −1 frame (MMTV). Similarly, MLVPK and MMTV elements were introduced into the NotI site of pcTET2 β wt GAP and pcTET2 β wt GAP AdML (Singh et al., 2008).

Cell Culture and Extracts for mRNP Purification and Immunoprecipitation

293T cells maintained in DMEM supplemented with 10% fetal bovine serum and antibiotics were used for mRNP purification experiments. Transfection by calcium phosphate was performed as described (Hogg and Collins, 2007a, 2007b). Harvested cell pellets were resuspended in hypotonic lysis buffer (HLB; 20 mM HEPES pH 7.6, 2 mM $MgCl_2$, 10% glycerol, 1 mM DTT, supplemented with protease inhibitors), subjected to freeze-thaw lysis, and extracted in 150 mM NaCl as described (Hogg and Collins, 2007a, 2007b). Where indicated, cells were treated with 100 μg/ml cycloheximide (Sigma) or 100 μg/ml puromycin (Sigma) for 4 hr prior to cell harvest.

Analysis of mRNP Composition by Mass Spectrometry

For mass spectrometry, complexes eluted in ammonium bicarbonate were dried under vacuum centrifugation and resuspended in SDS-PAGE sample buffer prior to electrophoresis. Proteins were identified by colloidal Coomassie staining (Sigma), and gel slices were excised for analysis. Mass spectrometry was performed at the Protein Core Facility at Columbia University by lc-ms/ms using a hybrid high-resolution quadrupole time-of-flight electrospray mass spectrometer. Results were analyzed using MASCOT software (Matrix Science).

RNase H Cleavage and Immunoprecipitation

293T cell extracts were prepared and supplemented as described for mRNP affinity purifications. RNase H guide oligonucleotides used were 5′-GTC ATT GGT CTT AAA-3′ (position 7), 5′-ACT GGT ACT AGC TTG-3′ (position 211), and 5′-CAT CCA TTC CAT GCA-3′ (position 305). Prior to immunoprecipitation, oligonucleotides were added to extracts at 10 μM final concentration, and endogenous RNase H was allowed to cleave for 1 hr at 4°C. Extracts were adjusted to contain 600 mM NaCl, 0.5% sodium deoxycholate, 0.5% NP-40, and 0.1% SDS to inhibit RNase H activity and promote dissociation of 5′ and 3′ fragments of mRNPs. Goat anti-Upf1 antibody (Santa Cruz) or nonspecific goat IgG (Sigma) prebound to Protein G Dynabeads (Invitrogen) were incubated in extracts for 1 hr, followed by extensive washing. Bound RNA and protein were eluted from beads in LDS sample buffer (Invitrogen). Immunoprecipitation experiments in Figure S1 were performed in HLB150 + 0.1% NP-40 throughout.

RNA Decay and Accumulation Assays

HeLa Tet-off Advance cells (Clontech) maintained in DMEM supplemented with 10% FBS and 2 ng/ml doxycycline (Sigma) were transfected in 60 mm plates using FuGENE 6 (Roche), according to the manufacturer's instructions. For each plate, 800 ng of the indicated pcTET2 β-globin plasmid was co-transfected with 200 ng pcβwtβ and 1000 ng pcDNA3.1 empty vector (Lykke-Andersen et al., 2000; Singh et al., 2008). Cells were split into four equal aliquots in 12-well plates 24 hr post-transfection. The next day, cells were washed with 1 ml PBS and incubated in medium without doxycycline for 4 hr (Figure 5) or 6 hr (Figure S4). Transcription was quenched by adding 1 μg/ml doxycycline, and cells were harvested in Trizol (Invitrogen) after 30 min and at the indicated intervals

thereafter. For accumulation assays (Figure 6), cells were transfected in the presence of 50 ng/ml tetracycline and harvested 6 hr after tetracycline was removed.

Detection of RNA and Protein

RNA was isolated using Trizol (Invitrogen) and resolved on formaldehyde/agarose gels. An end-labeled oligonucleotide probe against the PP7 tag cassette or random-primed probes were used for detection of mRNAs. Random-primed probes were derived from the HindIII-XbaI fragment of pcDNAGFPTP, the EcoRV-HindIII fragment of the HIV 3′LTR, and the HindIII-BamHI fragment of pcTET2βwtβ. Northern blots were imaged on a Typhoon Trio and quantification was performed using ImageQuant software (G.E.). Immunoblots were imaged on the Odyssey Infrared Imaging System (LI-COR), using donkey anti-rabbit and donkey anti-goat secondary antibodies conjugated to IRDye 800 (Rockland Immunochemicals) and donkey anti-mouse conjugated to IRDye 680 (LI-COR). Primary antibodies used for immunoblotting were rabbit anti-Upf1 (Santa Cruz); mouse anti-PABPC1 (Abcam), goat anti-Upf2 (Santa Cruz), and rabbit anti-SMG-1 (Abcam). Luciferase activity and GFP fluorescence in extracts were quantified using a POLARstar Omega multi-mode plate reader (BMG Labtech).

SUPPLEMENTAL REFERENCES

Babendure, J.R., Babendure, J.L., Ding, J.H., and Tsien, R.Y. (2006). Control of mammalian translation by mRNA structure near caps. RNA *12*, 851–861.

Girard, M., and Baltimore, D. (1966). The effect of HeLa cell cytoplasm on the rate of sedimentation of RNA. Proc. Natl. Acad. Sci. USA *56*, 999–1002.

Grentzmann, G., Ingram, J.A., Kelly, P.J., Gesteland, R.F., and Atkins, J.F. (1998). A dual-luciferase reporter system for studying recoding signals. RNA *4*, 479–486.

Li, M.Z., and Elledge, S.J. (2007). Harnessing homologous recombination in vitro to generate recombinant DNA via SLIC. Nat. Methods *4*, 251–256.

Lykke-Andersen, J., Shu, M.D., and Steitz, J.A. (2000). Human Upf proteins target an mRNA for nonsense-mediated decay when bound downstream of a termination codon. Cell *103*, 1121–1131.

Penman, S., Vesco, C., and Penman, M. (1968). Localization and kinetics of formation of nuclear heterodisperse RNA, cytoplasmic heterodisperse RNA and polyribosome-associated messenger RNA in HeLa cells. J. Mol. Biol. *34*, 49–60.

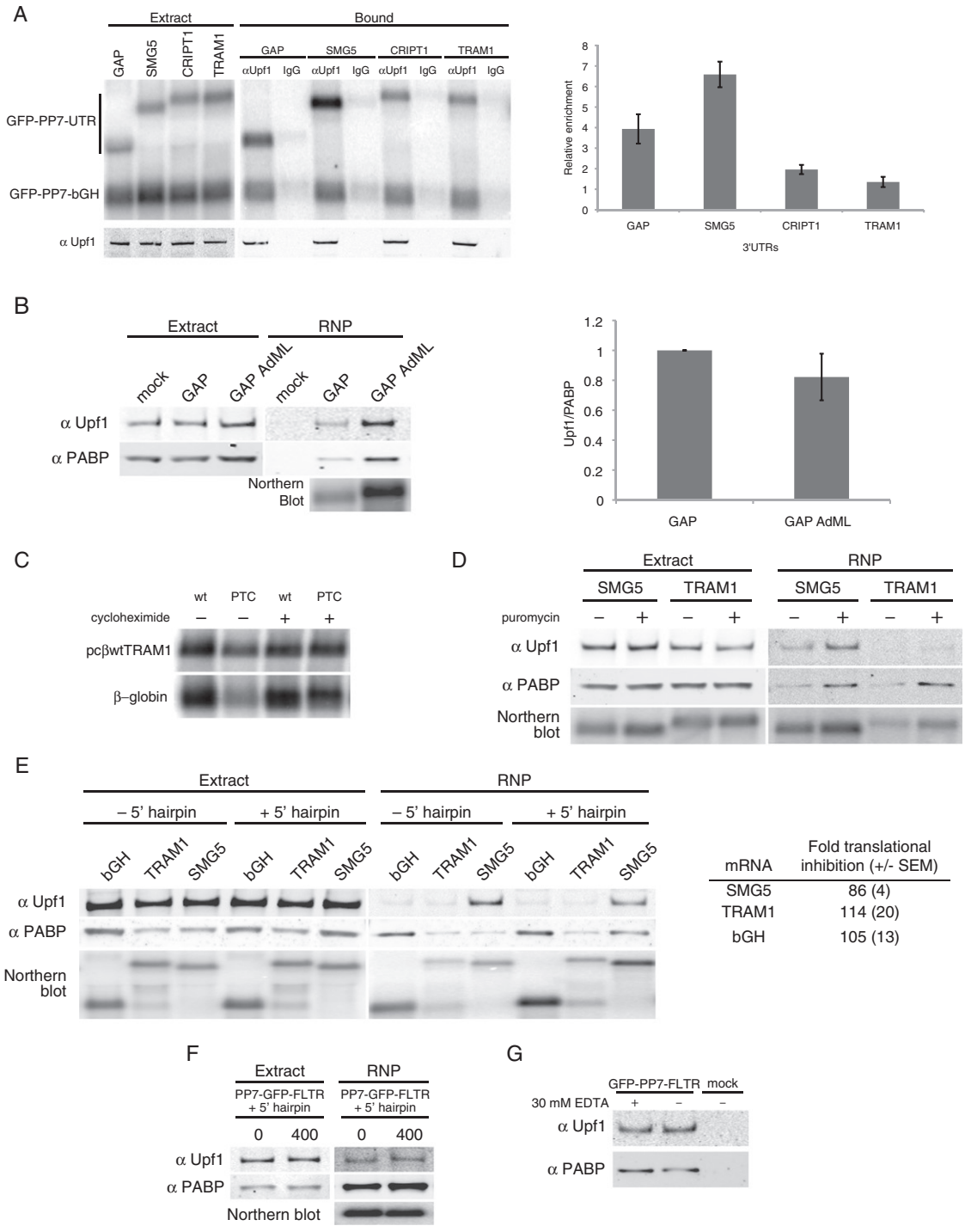

Figure S1. Preferential Accumulation of Upf1 on Specific mRNAs Is Independent of Translation and Ongoing NMD, Related to Figure 2 and Figure 3

(A) Antibodies against endogenous Upf1 preferentially coimmunoprecipitate mRNAs containing 3′UTRs known to specify NMD. 293T cells were cotransfected with constructs encoding the indicated 3′-tagged GFP mRNAs and, as an internal standard, a construct expressing tagged GFP mRNA containing the bovine growth hormone polyadenylation element (bGH). (Left) An anti-Upf1 antibody or nonspecific goat IgG was used for immunoprecipitation, and mRNA recovery was monitored by northern blotting with a probe against GFP sequences. Upf1 protein in extracts and in immunopurified material was detected using a rabbit anti-Upf1 antibody (bottom). (Right) Quantification of mRNA coimmunoprecipitation. Recovery of the indicated mRNAs was normalized to mRNA abundance in starting extracts, using the bGH-containing mRNA as an internal control. Error bars indicate ± SEM; n = 3.

(B) The presence of a spliced intron downstream of the TC does not alter Upf1 recruitment to mRNPs. Proteins in whole-cell extracts of transfected 293T cells

(Extract) or copurifying with tagged RNAs (RNP) were detected by immunoblotting with antibodies against endogenous Upf1 (top) or PABPC1 (middle). PP7-tagged GFP mRNAs contained the artificial GAP 3′UTR with (GAP AdML) or without (GAP) the adenovirus major-late intron. RNA recovery was assessed by northern blotting (bottom). (Right) Quantification of Upf1 association with the indicated mRNAs, normalized to copurifying PABPC1. Error bars indicate ± SEM; n = 2.

(C) Cycloheximide treatment inhibits NMD. 293T cells transiently expressing a control TRAM1 3′UTR-containing β-globin mRNA (pcβwtTRAM1; Singh et al., 2008) and either wild-type (pcβwtβ) or PTC-containing β-globin mRNAs (pcβ39β; Lykke-Andersen et al., 2000) were treated with 100 μg/ml cycloheximide for 4 hr prior to cell harvest as in Figure 3B. Stabilization of PTC-containing mRNAs by cycloheximide treatment was monitored by northern blotting.

(D) Transcript-specific accumulation of Upf1 in mRNPs persists following puromycin treatment. 293T cells transiently transfected with PP7-tagged GFP mRNAs containing the TRAM1 or SMG5 3′UTRs were treated (+) or not treated (−) with puromycin for 4 hr prior to cell harvest. Immunoblotting and northern blotting were performed as in (B). As a control to demonstrate puromycin activity, we observed that identical puromycin treatment abrogated differences in Upf1 copurification with mRNAs undergoing differential readthrough. See Figure S2C.

(E) Upf1 associates with poorly translated mRNAs. A stable hairpin structure previously shown to robustly inhibit translation initiation was inserted immediately downstream of the transcriptional start sites of constructs expressing 3′-tagged GFP mRNAs containing the indicated 3′UTRs (Babendure et al., 2006). Copurification of Upf1 and PABP with affinity-purified mRNPs lacking (− 5′ hairpin) or containing (+ 5′ hairpin) the initiation-inhibiting structure was monitored by immunoblotting as in (B). (Right) GFP fluorescence in extracts from cells expressing standard and hairpin-containing tagged RNAs was monitored using a POLARstar Omega multi-mode fluorescence plate reader. GFP signal in extracts was normalized to mRNA levels as determined by northern blotting. Fold translational inhibition is expressed as a ratio between normalized GFP levels from standard and hairpin-containing mRNAs (n = 2). Under conditions of ~100-fold translational inhibition, Upf1 continued to preferentially accumulate to higher levels on mRNAs containing the SMG5 3′UTR than mRNAs containing the bGH element or the TRAM1 3′UTR.

(F) Inhibition of translation initiation causes Upf1 accumulation to become insensitive to termination codon position. Stable hairpins were inserted at the 5′ end of constructs containing the GFP ORF in frame with the *nef* ORF of the HIV 3′LTR (Figure 2C). Corresponding experiments shown in Figure 2C demonstrated that mRNAs containing a TC at the end of the GFP ORF (TC position 0) copurified higher levels of Upf1 than mRNAs containing a TC at the 3′ end of the Nef ORF (400). In contrast, when translation initiation was inhibited due to a stable 5′ hairpin structure, the position of the TC did not affect Upf1 co-purification with mRNAs (+5′ hairpin, compare 0 and 400 samples).

(G) EDTA treatment does not disrupt Upf1 association with mRNPs. As indicated, mRNPs were washed extensively with standard HLB150 + 0.1% NP-40 buffer or buffer containing 30 mM EDTA, a concentration well established to efficiently dissociate 80S ribosomes (Penman et al., 1968; Girard and Baltimore, 1966). Identical results were obtained when EDTA was included throughout the purification (data not shown). Copurifying Upf1 and PABP were detected by immunoblotting as described.

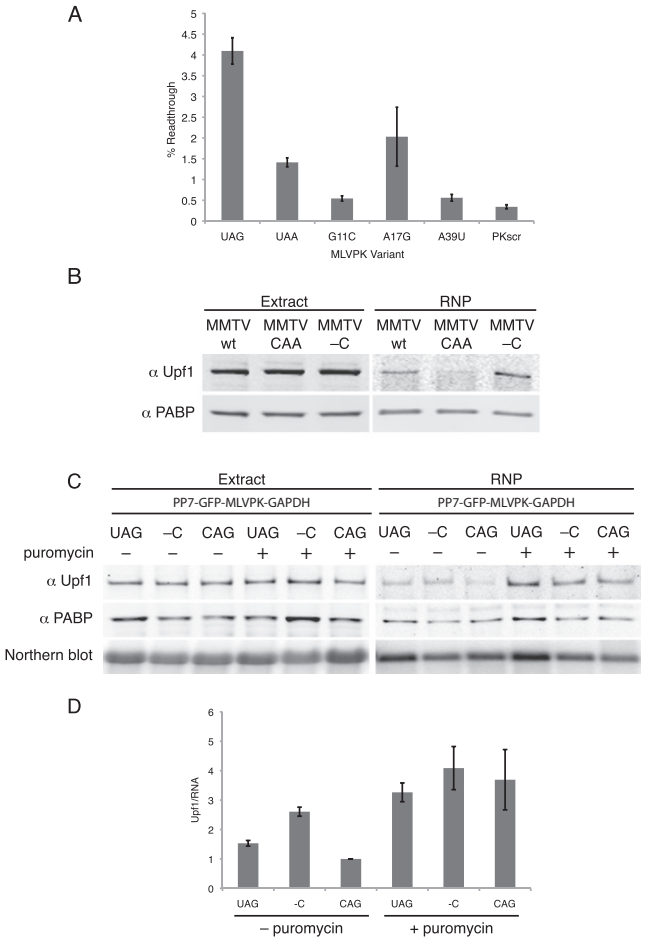

Figure S2. Retroviral Elements Reduce Upf1 Association with Long 3′UTR-Containing mRNAs, Related to Figure 4

(A) The efficiency of readthrough supported by the MLVPK variants used in this study was determined using a modification of an established bicistronic dual-luciferase assay (Grentzmann et al., 1998). Plasmids encoding *Renilla* and firefly luciferase ORFs separated by the indicated MLVPK variants or a scrambled pseudoknot sequence containing a termination codon (PKscr) were transfected into HeLa Tet-off cells, and dual luciferase assays were performed 48 hr after transfection. A construct lacking a termination codon was used to establish the ratio of *Renilla*:firefly luciferase activity generated by 100% readthrough, which served as the basis for calculating % readthrough. Error bars indicate ± SEM; n = 3.

(B) Repression of Upf1 recruitment to mRNPs by the Mouse mammary tumor virus −1 frameshifting element (MMTV −1FS). PP7-tagged RNAs containing the GFP ORF followed by the indicated MMTV −1FS variants and the intronless GAP artificial 3′UTR such that the GAPDH ORF was in the −1 reading frame were used for RNP isolation as described in the main text. Frameshifting by the wild-type MMTV element thus resulted in readthrough of the GFP TC and termination at the downstream GAPDH TC. As controls, mutations in the MMTV −1FS slippery sequence were used to ensure constitutive readthrough to the GAPDH TC (MMTV CAA) or constitutive termination at the upstream TC (MMTV −C). Whole-cell extracts and purified material were immunoblotted and probed with the indicated antibodies.

(C) Puromycin treatment abrogates the effects of readthrough-promoting elements on Upf1 accumulation in mRNPs. 293T cells expressing the indicated tagged RNAs (see also Figure 4) were allowed to grow under normal conditions (− puromycin) or in the presence of 100 μg/ml puromycin (+ puromycin) prior to extract preparation. Proteins copurifying with affinity-purified mRNPs were analyzed as in (B).

(D) Quantification of data in (C). Upf1 copurification with the indicated mRNAs was normalized to purified RNA levels. Normalized Upf1 levels were arbitrarily set to 1 for the untreated constitutive-readthrough control (CAG) RNA. Error bars indicate ± SEM; n = 2.

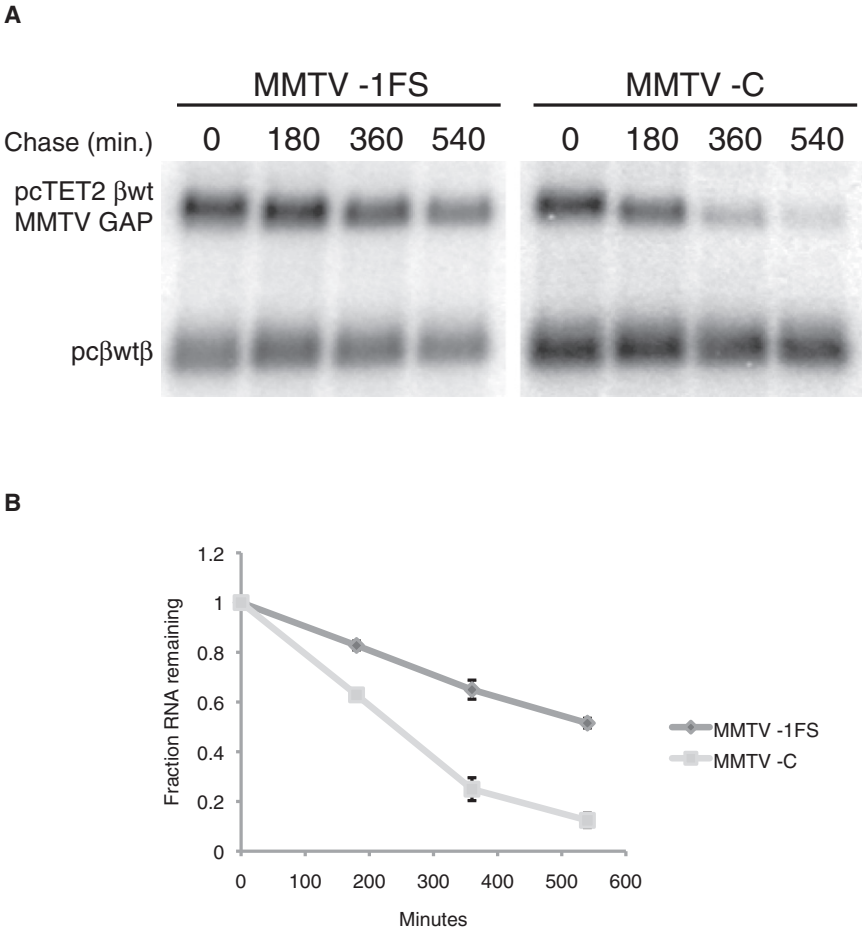

Figure S3. The MMTV −1 Frameshfting Element Stabilizes Targets of Decay, Related to Figure 5

(A) Decay assays of reporter mRNAs containing MMTV −1 frameshift element variants were performed as described in the main text. Constructs contained the β-globin ORF and the GAPDH ORF in the −1 frame, with intervening MMTV −1FS sequence. The MMTV wt sequence causes efficient −1 frameshifting, while the MMTV −C sequence lacks a functional slippery sequence and terminates constitutively at the upstream TC. Constructs encoding tet-regulated transcripts (pcTET2 βwt MMTV GAP; top band) were transiently transfected in HeLa Tet-off cells, along with the constitutively expressed wild-type β-globin reporter (pcβwtβ; bottom band). RNA was harvested 30 min after transcription was halted and at 3 hr intervals thereafter.

(B) Quantification of the data in (A). Error bars indicate ± SEM; n = 3.

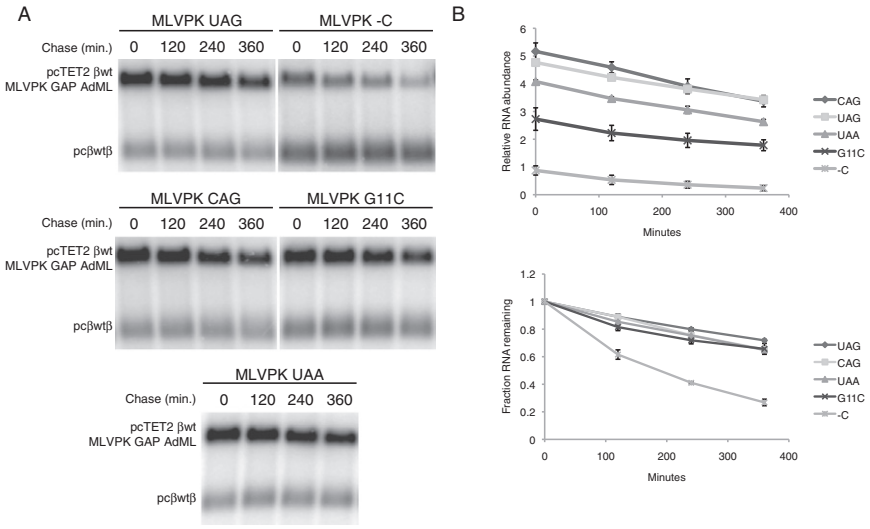

Figure S4. MLVPK Variants Stabilize Reporter mRNAs with the GAP AdML Intron-Containing 3′UTR, Related to Figure 6

(A) Constructs encoding the tet-regulated AdML-intron-containing transcripts (pcTET2 βwt MLVPK GAP AdML, top bands) were cotransfected with the constitutively expressed wild-type β-globin reporter (pcβwtβ; bottom bands) in HeLa Tet-off cells. RNA was harvested 30 min after transcription was halted by addition of doxycycline and at 2 hr intervals thereafter.

(B) Quantification of decay assays. (Top) Levels of tet-regulated reporter mRNAs were normalized to levels of the wild-type β-globin transfection control. (Bottom) RNA levels at the initial time point were arbitrarily set to 1, facilitating visualization of decay. Error bars indicate ± SEM; n = 3. Assaying RNA accumulation levels reveals the contribution of decay that occurs rapidly following transcript synthesis. The differences in accumulation of RNAs undergoing various levels of readthrough are likely due to enhanced decay during the transcription pulse and the interval between doxycycline addition and RNA extraction. These data are consistent with the expectation that any enhancement of decay by the EJC should occur prior to the first readthrough event, which disrupts the EJC and stabilizes mRNAs over the assay time course.